THE JOURNAL OF PHYSICAL CHEMISTRY C

Article

pubs.acs.org/JPCC

Molecular-Level Understanding of CeO_2 as a Catalyst for Partial Alkyne Hydrogenation

Javier Carrasco,*[,†,‡] Gianvito Vilé,[§] Delia Fernández-Torre,[∥,⊥] Rubén Pérez,[∥,#] Javier Pérez-Ramírez,*[,§] and M. Verónica Ganduglia-Pirovano[†]

[†]Instituto de Catálisis y Petroleoquímica, CSIC, C/Marie Curie 2, 28049 Madrid, Spain

[‡]CIC Energigune, Albert Einstein 48, 01510 Miñano (Álava), Spain

[§]Institute for Chemical and Bioengineering, Department of Chemistry and Applied Biosciences, ETH Zurich, Vladimir-Prelog-Weg 1, 8093 Zurich, Switzerland

[∥]Departamento de Física Teórica de la Materia Condensada, Universidad Autónoma de Madrid, 28049 Madrid, Spain

[⊥]Instituto de Estructura de la Materia, CSIC, Serrano 121, 28006 Madrid, Spain

[#]Condensed Matter Physics Center (IFIMAC), Universidad Autónoma de Madrid, 28049 Madrid, Spain

Supporting Information

ABSTRACT: The unique catalytic properties of ceria for the partial hydrogenation of alkynes are examined for acetylene hydrogenation. Catalytic tests over polycrystalline CeO_2 at different temperatures and H_2/C_2H_2 ratios reveal ethylene selectivities in the range of 75−85% at high degrees of acetylene conversion and hint at the crucial role of hydrogen dissociation on the overall process. Density-functional theory is applied to $CeO_2(111)$ in order to investigate reaction intermediates and to calculate the enthalpy and energy barrier for each elementary step, taking into account different adsorption geometries and the presence of potential isomers of the intermediates. At a high hydrogen coverage, β-C_2H_2 radicals adsorbed on-top of surface oxygen atoms are the initial reactive species forming C_2H_3 species effectively barrierless. The high alkene selectivity is owed to the lower activation barrier for subsequent hydrogenation leading to gas-phase C_2H_4 compared to that for the formation of β-C_2H_4 radical species. Moreover, hydrogenation of C_2H_5 species, if formed, must overcome significantly large barriers. Oligomers are the most important byproduct of the reaction and they result from the recombination of chemisorbed C_2H_x species. These findings rationalize for the first time the applicability of CeO_2 as a catalyst for olefin production and potentially broaden its use for the hydrogenation of polyunsaturated and polyfunctionalized substrates containing triple bonds.

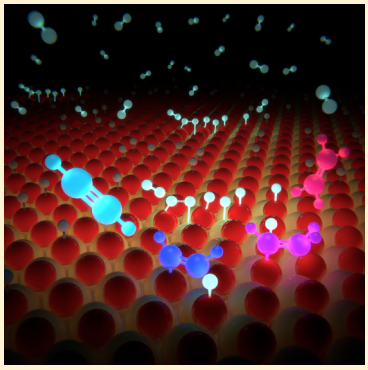

1. INTRODUCTION

The partial hydrogenation of alkynes to alkenes is a crucial step for the purification of olefin streams in the petrochemical industry as well as for the manufacture of fine chemicals.[1,2] To this end, a high degree of product selectivity is required. Prototypical heterogeneous catalysts to perform this reaction are based on palladium.[3] This metal is highly active at moderate temperature and hydrogen pressure but often suffers from suboptimal selectivity and lifetime due to alkane and oligomer formation.[4−6] For this reason, the development of novel materials excelling the performance of palladium-based systems constitutes a key challenge requiring identification of active sites and molecular-level understanding of the associated reaction mechanism.[6−10]

The recent discovery that CeO_2 exhibits a remarkable selectivity in the partial gas-phase hydrogenation of alkynes[11] has opened exciting perspectives in catalysis research. In the past, ceria was applied in the formulation of various alkyne and alkadiene hydrogenation catalysts, acting as a promoter or stabilizer and most commonly as a carrier of noble metal nanoparticles.[12−14] However, its stand-alone ability to catalyze these reactions has never been stated before. With a propene selectivity of 91% at ca. 100% propyne conversion,[11] ceria is one of the most effective catalysts ever reported for this family of reactions. In contrast to that, other reducible oxides such as TiO_2 and ZnO were inactive in the gas-phase hydrogenation of alkynes under similar conditions.[11] A high surface area and the absence of oxygen vacancies are beneficial for attaining high catalytic performances. Additionally, a large hydrogen excess in the feed mixture and temperatures above 473 K are required, strongly suggesting that hydrogen splitting is the rate-limiting step. These results have been recently confirmed and generalized for the partial hydrogenation of other functional groups, including substituted nitroarenes.[15] However, a sound mechanistic insight into partial hydrogenation by ceria, which includes the determination of the relevant reaction pathways, does not yet exist. This knowledge is vital to rationalize the

Received: November 20, 2013
Published: January 14, 2014

   dx.doi.org/10.1021/jp410478c | J. Phys. Chem. C 2014, 118, 5352−5360

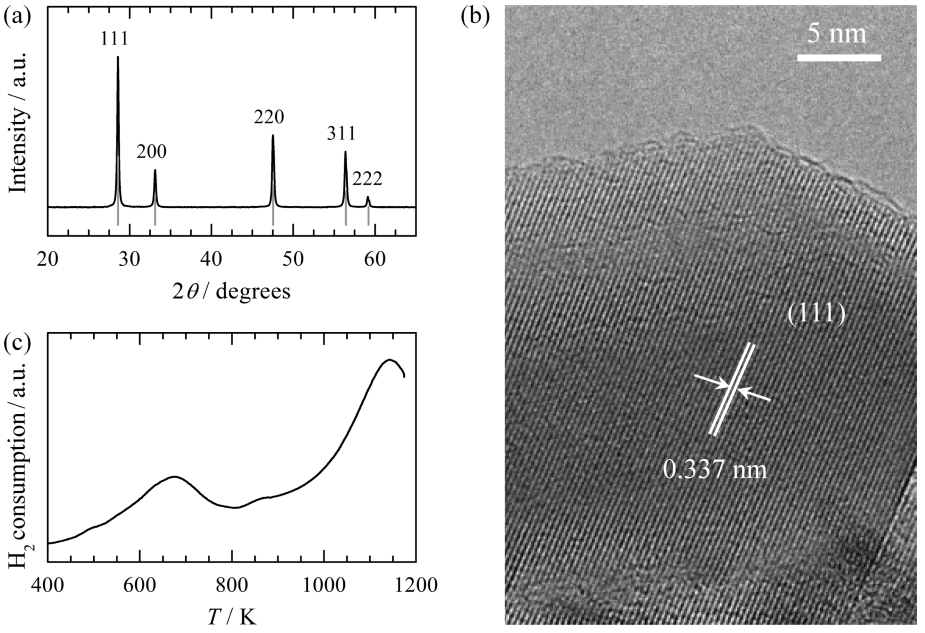

Figure 1. XRD pattern (JCPDS 65-5923 as reference in gray) (a), HRTEM micrograph (b), and H_2-TPR profile of the CeO_2 catalyst (c).

origin and uniqueness of the highly selective character of CeO_2 for olefin production as well as to devise its potential applicability for the liquid-phase hydrogenation of polyfunctionalized substrates containing triple bonds.

In this work, we focus on elucidating the mechanism for the partial (and full) hydrogenation of acetylene to ethylene (and ethane) over the pristine—most stable and exposed[16,17]—CeO_2(111) surface. Ethylene stands at the basis of the chemical industry and is involved in the production of a wide range of solvents, raw materials for paints, elastomers, thermoplastics, and synthetic fibers. Our catalytic experiments over polycrystalline CeO_2 indeed confirm that the reaction rate increases quasi-linearly with increasing the partial pressure of hydrogen, attaining an ethylene selectivity of up to 85%. Prereduction in H_2 flow of ceria affects the catalyst performance, decreasing the acetylene conversion and ethylene selectivity, which suggests that potential sites for the adsorption of reactants and intermediates were reduced during this pretreatment. Density-functional theory (DFT) calculations were performed in order to investigate the intermediate species of the reaction and to calculate the reaction enthalpy and energy barrier for each elementary step. Despite the innumerable theoretical studies modeling metal surfaces (mostly Pd, Ni, Cu, Au, Ag, and Ni–Zn)[8,9,18−22] for alkyne hydrogenation, no investigations over metal oxides, and specifically reducible oxides such as ceria, has been yet attempted in hydrogenation catalysis. In addition, finding the minimum energy structures of intermediates adsorbed on CeO_2 with respect to both the localization of excess electrons that appear upon reduction and the character of the 4*f* state associated to each Ce^{3+} ion still represents a challenge in the theoretical modeling of reduced ceria systems using DFT.[23−32] The ab initio approach presented here provides an explanation of the selective character of ceria in hydrogenation of triple bonds.

2. EXPERIMENTAL SECTION

Materials and Catalyst Characterization. Commercial CeO_2 nanopowder (Aldrich, ref: 544841) of high purity with a nominal total surface area of 70 $m^2\ g^{-1}$ was calcined in static air at 673 K for 5 h and eventually prereduced in flowing hydrogen (42 $cm^3\ min^{-1}$, 5 vol.% H_2/He) at 673 K for 30 min (heating rate = 5 K min^{-1}). Powder X-ray diffraction (XRD) was acquired in a PANalytical X'Pert PRO-MPD diffractometer equipped with Bragg–Brentano geometry and Ni-filtered Cu Kα radiation (λ = 0.1541 nm). Data were recorded in the 2θ range of 5–70°, with an angular step size of 0.017° and a counting time of 0.26 s per step. Chemical composition analyses were carried out by inductively coupled plasma optical emission spectroscopy (ICP-OES) on a Horiba Ultra 2 instrument equipped with photomultiplier tube detection. High-resolution transmission electron microscopy (HR-TEM) was undertaken on a FEI Tecnai F30 microscope operated at 300 kV. Temperature-programmed reduction in hydrogen (H_2-TPR) was carried out in a Thermo TPD/R/O 1100 unit equipped with a thermal conductivity detector. The catalyst (ca. 50 mg) was loaded in the quartz microreactor (11 mm i.d.), pretreated in helium (20 $cm^3\ min^{-1}$) at 473 K for 30 min, and cooled down to 323 K in He. The analysis was carried out in 5 vol.% H_2/N_2 (20 $cm^3\ min^{-1}$), ramping the temperature from 323 to 1173 at 5 K min^{-1}. Fourier transform infrared (FTIR) spectroscopy was performed in a Bruker Optics Vertex 70 spectrometer equipped with high-temperature cell, ZnSe windows, and mercury–cadmium–telluride (MCT) detector. The cell was filled with the powder catalyst and carefully leveled off to reduce reflections off the sample surface and to ensure reproducible results. The spectra were recorded in the range of 650–4000 cm^{-1}, by coaddition of 200 scans at a nominal resolution of 4 cm^{-1}. The amount of oxygen vacancies was determined from the absorbance at 3640 cm^{-1}.[11]

Catalytic Tests. The gas-phase hydrogenation of acetylene was carried out in a continuous-flow fixed-bed microreactor (12 mm i.d.) at ambient pressure using 0.56 g of catalyst (particle size = 0.2–0.4 mm). The partial C_2H_2 pressure was kept constant at 25 mbar; the contact time (τ = volume of catalyst bed/total volumetric flow), temperature, and partial H_2 pressure were varied in the range of 0.12–1 s, 423–623 K, and 250–750 mbar (H_2/C_2H_2 = 10–30), respectively, using He as the balance gas. All the catalytic data were measured

dx.doi.org/10.1021/jp410478c | J. Phys. Chem. C 2014, 118, 5352–5360

under steady-state conditions and the performance was stable for several hours on stream. The fulfillment of relevant criteria was verified in order to discard mass-transport limitations. In addition, the temperature gradients along the bed, measured as the difference between the temperature at the outlet of the bed and the oven temperature, were <5 K, enabling quasi-isothermal operation. The composition of the gas at the reactor outlet was analyzed by an online gas chromatograph (Agilent GC7890A) equipped with a GS-GasPro column and a flame ionization detector. The conversion of acetylene, $X(C_2H_2)$, was determined as the amount of reacted alkyne divided by the amount of alkyne at the reactor inlet. The turnover frequency was expressed as millimole of C_2H_4 produced per mole of surface oxygen (active sites) per unit of time. The moles of surface oxygen were calculated as the product of the mass of the catalyst multiplied by the surface oxygen density and by the surface area, and divided by the Avogadro number. Particularly, the surface oxygen density in polycrystalline CeO_2 was calculated taking into account the density of surface oxygen on each facet and their relative abundance in the XRD pattern (Figure 1a), assuming that all faces contribute equally to the activity of CeO_2. The selectivity to ethylene, $S(C_2H_4)$, and ethane, $S(C_2H_6)$, were calculated as the quantity of product formed divided by the amount of converted alkyne. The selectivity to oligomers was determined as $S(OL) = 1 - S(C_2H_4) - S(C_2H_6)$.

3. THEORETICAL METHODS

Spin-polarized DFT and supercell periodic models were used as implemented in the Vienna ab initio simulation package (VASP).[33−35] We treated explicitly the C (2s, 2p), O (2s, 2p), and Ce (4f, 5s, 5p, 5d, 6s) electrons as valence states expanded in plane-waves with a cutoff energy of 400 eV, whereas the remaining electrons were replaced by Perdew−Burke−Ernzenhof (PBE)-based projector-augmented wave (PAW) potentials.[36] Total energies and electron densities were computed using the DFT+U approach of Dudarev et al.,[37] in which a Hubbard U-like term describing the onsite Coulomb interactions ($U_{eff} = U - J$, that is, the difference between the Coulomb U and exchange J parameters, hereinafter referred to as simply U) is added to the PBE generalized-gradient approximation (GGA) functional.[38] We used a value of U = 4.5 eV for Ce atoms, which was calculated self-consistently by Fabris et al.[39] using a linear response approach.[40] A Monkhorst−Pack[41] grid with 6 × 6 × 1 k-point sampling per (1 × 1) surface unit cell was used.

The O-terminated $CeO_2(111)$ surface with (3 × 3) periodicity was modeled using a supercell, containing six atomic layers separated by at least 12 Å of vacuum. All the atoms in the three bottom layers of the slab were fixed at their PBE+U bulk-truncated (a_{ceria} = 5.485 Å) positions during geometry optimization, whereas the rest of atoms were allowed to fully relax. The calculations of gas-phase species (H_2, C_2H_2, C_2H_4, and C_2H_6) were performed with Γ-point sampling using at least 12 × 12 × 12 $Å^3$ boxes. For all the systems investigated, a range of different initial positions and orientations was considered, and the structures were relaxed using a conjugate-gradient algorithm with a residual force threshold of 0.05 eV $Å^{-1}$. All reported adsorption energies were calculated in relation to the corresponding gas-phase molecule and the bare $CeO_2(111)$ surface, implying that negative reaction energies correspond to exothermic processes. We found that the adsorption of H or C_2H_x species on the $CeO_2(111)$ surface results in the formation of one Ce^{3+} ion per adsorbed species. It is known that such Ce^{3+} ions are likely to be more stable on the first cationic layer of the $CeO_2(111)$ surface.[23,29−32] Imposing this as a constrain, we systematically explored a range of possible configurations for the location of Ce^{3+} ions upon adsorption of a given species. This search revealed relative energy differences between the global minima and other possible locations of Ce^{3+} ions as large as 130 meV/Ce^{3+}, i.e., up to 390 meV when a maximum of three Ce^{3+} ions are present (Figure S1 in Supporting Information). Consequently, all minima reported in the following correspond to the lowest-energy Ce^{3+} ion configurations found. To determine the electronic ground state we used a self-consistent-field minimization algorithm as applied in ref 25 and acknowledge the challenge for DFT+U to find the global minimum with respect to 4f orbital occupations. We noticed that only high-spin (ferromagnetic-like) states were considered for the sake of simplicity. This assumption is reasonable, since the energy difference between the high-spin state and any other spin state is very small, typically less than 10 meV.

Vibrational frequencies were obtained numerically by building the Hessian dynamical matrix through finite atomic displacements of 0.01 Å from the optimized structures. After diagonalization of the Hessian matrix, the corresponding harmonic frequencies associated to each normal vibrational mode were obtained.

Transition structures (TS) for the considered reaction paths were located by employing the nudged elastic band (NEB) algorithm[42] using at least five images along each pathway. Harmonic vibrational frequency analysis showed that all TS structures had only one imaginary frequency.

4. RESULTS AND DISCUSSION

Characterization of CeO_2 and Hydrogenation Performance. The X-ray diffraction pattern in Figure 1a shows that CeO_2 is the only crystalline phase in the commercial sample. HR-TEM in Figure 1b shows that the ceria nanoparticles primarily expose (111) facets with an interplanar spacing of 0.337 nm. ICP-OES analyses confirmed the high purity of the sample, which contains no trace of conventional hydrogenation metals such as Pd, Pt, Au, and Ni. Catalytic tests assessing the influence of temperature and H_2/C_2H_2 ratio on the activity and selectivity were conducted (Figure 2). Raising the temperature from 423 to 623 K (Figure 2a), the acetylene conversion reached a maximum (84%) at 473−523 K. The lower conversion above 523 K was attributed to the detrimental effect of surface CeO_2 reduction,[11] which starts at 523 K (Figure 1c) and leads to the formation of oxygen vacancies (*vide infra*). The selectivity to ethylene slightly increases with the temperature, reaching 85% as the highest value. Despite the large hydrogen excess in the feed mixture (H_2/C_2H_2 = 30), the selectivity to ethane is remarkably low (<10%) and the selectivity to oligomers reaches up to 16%. Figure 2b shows the influence of the feed H_2/C_2H_2 ratio on the catalytic performance of ceria. The conversion of acetylene increases linearly with the inlet partial pressure of hydrogen, strongly suggesting that H_2 dissociation is rate limiting. At H_2/C_2H_2 = 30 and 523 K, the highest turnover frequency (TOF) was obtained, corresponding to 0.3 mmol C_2H_4 mol O^{-1} s^{-1}. This value is comparable to the intrinsic activity of Ag-based catalysts in hydrogenation.[22] The selectivity to ethylene increases from 73% at H_2/C_2H_2 = 10 to 80% at H_2/C_2H_2 = 20, and remains unchanged at a higher ratio. The selectivity to ethane did not

dx.doi.org/10.1021/jp410478c | J. Phys. Chem. C 2014, 118, 5352−5360

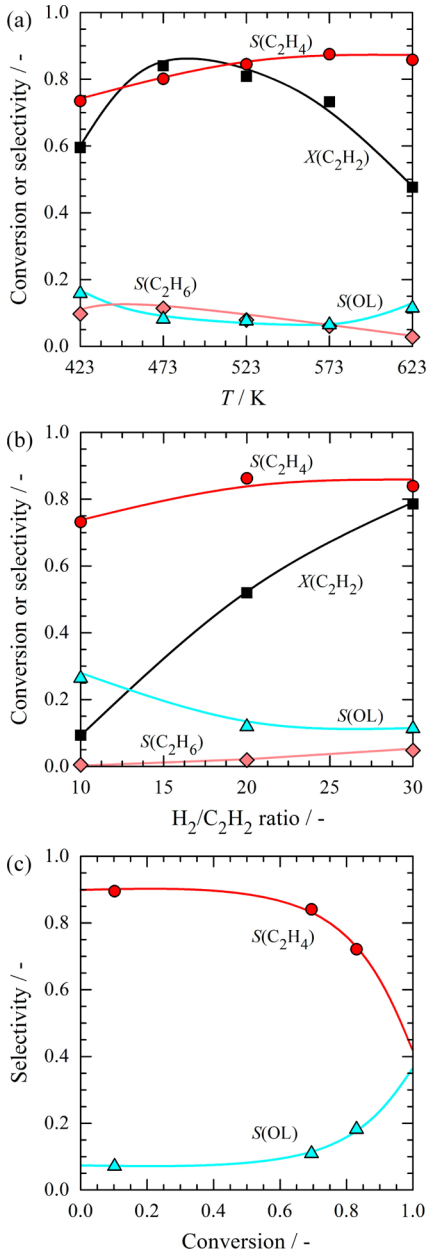

Figure 2. Acetylene hydrogenation performance of CeO_2 versus (a) temperature (at H_2/C_2H_2 = 30, τ = 0.35 s) and (b) H_2/C_2H_2 ratio (at T = 523 K, τ = 0.35 s), and (c) selectivity to ethylene and oligomers as a function of the acetylene conversion (at T = 523 K, H_2/C_3H_4 = 30, τ = 0.12−1 s). The experiments were conducted at 1 bar.

exceed 10%. At low hydrogen coverage ($H_2/C_2H_2 \leq 15$), extensive oligomerization takes place. At high coverage, the addition of hydrogen in the feed suppresses undesired pathways, pointing to a decisive role of H_2 dissociation in the reaction mechanism for maximizing the alkene production. Finally, upon increasing the conversion of acetylene at fixed T and H_2/C_2H_2 ratio (Figure 2c), a reduced selectivity to ethylene was observed, with the concomitant increase in oligomer formation. This result suggests that ethylene partakes in the oligomerization pathway. At optimal reaction conditions (T = 523 K, H_2/C_2H_2 = 30, τ = 0.35 s), a stable selectivity to ethylene of ca. 80% at a degree of acetylene conversion of ca. 80% was attained; this result excels the typical performance of conventional hydrogenation catalysts (typically, at a similar degree of conversion, the ethylene selectivity is 50−75%).[3,6,9,43]

The influence of the presence of oxygen vacancies (formed by extensive prereduction of ceria in H_2 and quantified by infrared spectroscopy) on the catalytic performance is depicted in Figure 3. On the oxidic catalyst (no pretreatment in H_2 flow), a high acetylene conversion and ethylene selectivity have been attained. Upon prereduction of CeO_2 in 5 vol.% H_2/He at 673 K, oxygen vacancies are created, and a drop in the acetylene conversion and ethylene selectivity is observed. Therefore, this result points to the detrimental role of ceria reduction, suggesting that oxygen atoms are active centers for the adsorption of reactants and intermediates.

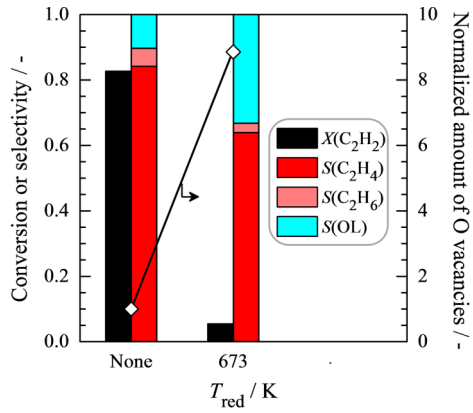

Figure 3. Influence of prereduction temperature of CeO_2 on the acetylene hydrogenation performance (at T = 523 K, H_2/C_2H_2 = 30, τ = 0.35 s, and P = 1 bar), and its effect on the formation of oxygen vacancies (open diamonds, determined by infrared spectroscopy and normalized to the amount of vacancies in 'None').

Acetylene Activation. The fact that ceria predominantly exposes (111) facets and nonreduced surfaces are beneficial for the hydrogenation of alkynes accounts for the choice of CeO_2(111) as the model catalytic surface.

The molecular adsorption of hydrocarbon molecules on CeO_2(111) is expected to be very weak and dominated by van der Waals dispersion forces. Indeed, the PBE+U adsorption of C_2H_2 on CeO_2(111) is only −0.10 eV. Furthermore, the adsorption of C_2H_2 as a radical species on-top of a surface oxygen atom is exothermic (−0.12 eV), with the unpaired electron localized on the β carbon[44] (Figure 4a). The electron removed from such β-C_2H_2 species yields to the formation of one Ce^{3+} ion. Radicals are generally short-lived and highly reactive. As discussed below, these species play a crucial role in the selective hydrogenation to C_2H_4 at high H_2 coverage. In addition, they are likely to promote the formation of oligomers at low H_2/C_2H_2 ratios.

Stronger binding can be achieved upon dissociation and, in particular, it has been proposed that C_3H_4 and other hydrocarbons dissociatively adsorb on CeO_2(111) via an heterolytic process through the formation of acetylide-like species on-top a surface cerium atom without ceria reduction.[11] In the case of C_2H_2, our PBE+U calculations show that dissociative heterolytic adsorption (Figure 4b) on CeO_2(111) is endothermic by 0.38 eV with respect to the gas-phase C_2H_2 molecule. Notwithstanding, dissociative homolytic adsorption is strongly exothermic (−1.77 eV) and, therefore, the adsorption mechanism for C_2H_2 on CeO_2(111) leads to the formation of an acetylide (H−C≡C) and a H species on top of two adjacent

dx.doi.org/10.1021/jp410478c | J. Phys. Chem. C 2014, 118, 5352−5360

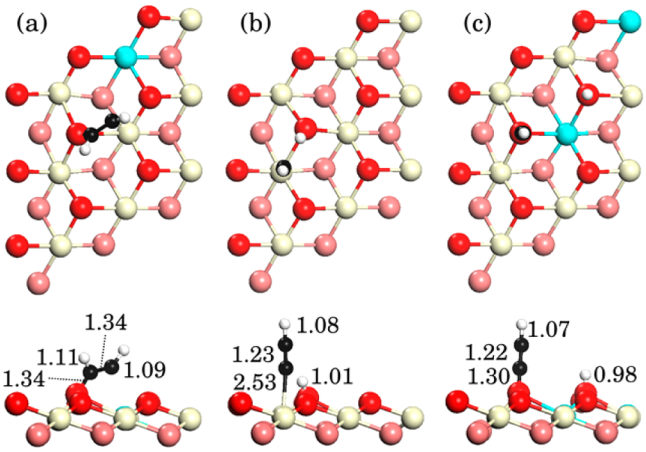

Figure 4. Top and side views of the lowest energy optimized structures for C_2H_2 adsorption on a (3 × 3) $CeO_2(111)$ surface via (a) β-C_2H_2 radical, (b) heterolytic, and (c) homolytic dissociation. The numbers indicate interatomic C−H, C−C, C−Ce, C−O, and O−H distances in Å. Red, light red, black, and white balls stand for surface O, subsurface O, C, and H atoms, respectively. Ce^{4+} and Ce^{3+} ions are cream and light blue, respectively. For clarity, only the top three atomic layers of the $CeO_2(111)$ surface are shown.

surface oxygen atoms (Figure 4c). Notice that unlike heterolytic dissociation, homolytic dissociation implies the reduction of ceria, resulting in the formation of two Ce^{3+} ions. The infrared spectra of C_2H_2 adsorbed on CeO_2 in Figure 5

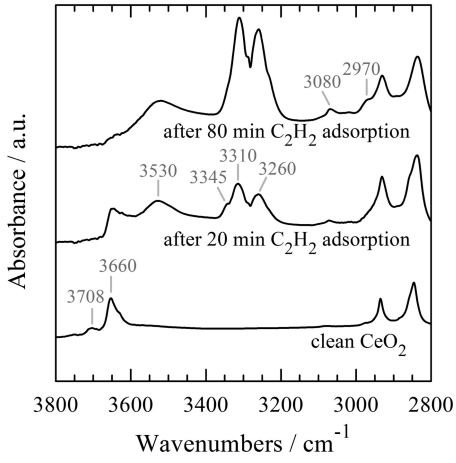

Figure 5. Infrared spectra of CeO_2 in He (20 cm^3 min^{-1}) and after 20 and 80 min of exposure to 5 vol% C_2H_2/He (20 cm^3 min^{-1}). The spectra were recorded at 523 K in the absence of gas-phase H_2.

provide further evidence for the homolytic dissociation pathway. After 20 min exposure time, the bands at 3708 cm^{-1} and 2160 cm^{-1} are assigned to the stretching modes of monocoordinated O−H and H−C≡C species, respectively. These experimental values agree well with the PBE+U values of such vibrational modes for the homolytic adsorption structure: 3702 cm^{-1} and 2153 cm^{-1}, respectively. Interestingly, after 80 min exposure time, the absorption at 3080 cm^{-1} gains intensity; this band is in reasonable good agreement with the computed O−H stretching mode for heterolytic adsorption (3110 cm^{-1}). This result suggests that at high coverage (longer exposure times), surface O sites become saturated and C_2H_2 might start to adsorb heterolytically on Ce sites.

Reaction Mechanism. The energy profile of acetylene hydrogenation on $CeO_2(111)$ determined by DFT is summarized in Figure 6, and a detailed list of all elementary steps with their corresponding reaction and activation energies can be found in Table 1. The elementary steps involved in the partial hydrogenation process are

$$C_2H_2 + 2H_2 + 2^* \rightarrow C_2H_2 + H_2 + H_2^* + * \quad (R1)$$

$$C_2H_2 + H_2 + H_2^* + * \rightarrow C_2H_2 + H_2 + (H,H)^* + * \quad (R2)$$

$$C_2H_2 + H_2 + (H,H)^* + * \rightarrow C_2H_2 + H_2 + 2H^* \quad (R3)$$

$$C_2H_2 + H_2 + 2H^* \rightarrow H_2 + (\beta\text{-}C_2H_2,H)^* + H^* \quad (R4)$$

$$H_2 + (\beta\text{-}C_2H_2,H)^* + H^* \rightarrow H_2 + C_2H_3^* + H^* \quad (R5)$$

$$H_2 + C_2H_3^* + H^* \rightarrow H_2 + (C_2H_3,H)^* + * \quad (R6)$$

$$H_2 + (C_2H_3,H)^* + * \rightarrow H_2 + C_2H_4 + 2^* \quad (R7)$$

Each asterisk denotes a clean $CeO_2(111)$ surface. Reactants, intermediates, and products that are followed by an asterisk stand for adsorbed species (our DFT structure optimizations show that the adsorption of all considered species takes place preferentially on top of surface O atoms). Species in parentheses and separated by commas indicate coadsorbed species on nearby active surface O sites.

We have arbitrarily assumed that H_2 physisorption and subsequent dissociation, eqs R1 and R2, are the initial steps instead of the adsorption of a gas-phase C_2H_2 molecule, eq R4. This assumption is actually meaningful because high acetylene conversion rates are *only* achieved under experimental conditions when H_2 is in high excess in relation to acetylene; indeed this is a strong indication that the dissociation of hydrogen is the limiting step of the whole process. Consequently, the reaction starts with the physisorption of H_2 (eq R1) followed by homolytic dissociative chemisorption to leave two H* species (eq R2) and release 2.35 eV. The two H atoms adsorb on top of two nearest neighbor surface O atoms to form two hydroxyl groups and two Ce^{3+} (Figure S2 in Supporting Information). This elementary step is hindered by an energy barrier of 1.00 eV.[45] Previous DFT+U calculations reported a much lower barrier (0.22 eV).[46] However, using their reported TS structure and their computational setup, we found the structure to be unstable. Nonetheless, this higher activation energy is compatible with the high H_2 pressures needed for conversion. The separation of two nearest neighbor H* species leading to two isolated species, (H,H)* → H* + H*, is thermodynamically slightly unfavorable by 0.07 eV (eq R3). The reaction continues with the adsorption of an acetylene molecule near to one hydroxyl group (eq R4) to form (β-C_2H_2,H)* (inset D in Figure 6). This step is energetically favored by only 0.15 eV. Then such radical species can readily react with the nearby hydroxyl group leading to the formation of a C_2H_3* and releasing 1.48 eV. In addition, this process has a barrier of only 0.09 eV. At this stage, the reaction can proceed toward the coadsorption of C_2H_3* and H* species via eq R6 and the formation and release of a gas-phase ethylene molecule (eq R7), resulting in an overall partial hydrogenation process. This last elementary step is substantially endothermic by 1.65 eV and presents a large energy barrier of 2.86 eV. Although this energy barrier for the formation of

dx.doi.org/10.1021/jp410478c | J. Phys. Chem. C 2014, 118, 5352−5360

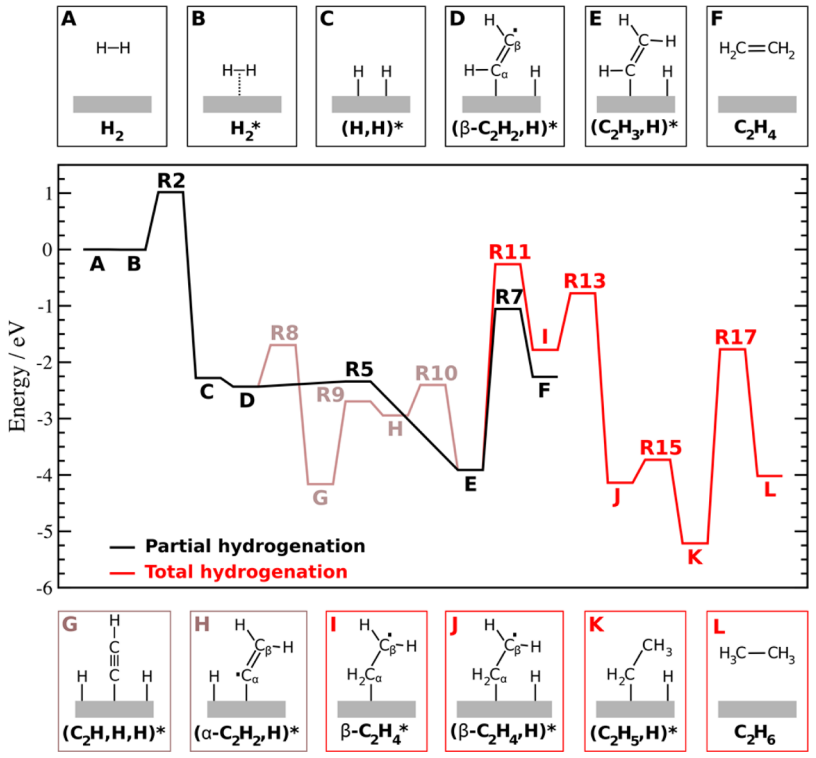

Figure 6. Reaction energy profile for acetylene hydrogenation on $CeO_2(111)$. All energies are referenced to the total energy of $H_2(g)$, $C_2H_2(g)$, and the clean $CeO_2(111)$ surface (state A). States A–L stand for minima and their structures are schematically shown in the insets, whereas transition structures are indicated by R2–R17 (see Figures S2–S5 for more details). Colors indicate different pathways: partial hydrogenation of acetylene to ethylene via R5 (black line) or via dissociative acetylene adsorption (light brown), and total hydrogenation to C_2H_6 (red line).

Table 1. Reaction Energies (E_r) and Activation Energies of Forward ($E_{a,f}$) and Backward ($E_{a,b}$) Reactions in eV for the Elementary Steps Involved in the Hydrogenation of Acetylene on $CeO_2(111)$

eq	reaction	E_r	$E_{a,f}$	$E_{a,b}$
R1	$H_2 + * \rightarrow H_2*$	0.00	-	-
R2	$H_2* \rightarrow (H,H)*$	−2.35	1.00	3.35
R3	$(H,H)* \rightarrow H* + H*$	0.07	-	-
R4	$H* + C_2H_2 \rightarrow (\beta\text{-}C_2H_2,H)*$	−0.15	-	-
R5	$(\beta\text{-}C_2H_2,H)* \rightarrow C_2H_3*$	−1.48	0.09	1.58
R6	$H* + C_2H_3* \rightarrow (C_2H_3,H)* + *$	0.01	-	-
R7	$(C_2H_3,H)* \rightarrow C_2H_4 + *$	1.65	2.86	1.20
R8	$(\beta\text{-}C_2H_2,H)* \rightarrow (C_2H,H,H)*$	−1.73	0.74	2.47
R9	$(C_2H,H,H)* \rightarrow (\alpha\text{-}C_2H_2,H)*$	1.22	1.47	0.25
R10	$(\alpha\text{-}C_2H_2,H)* \rightarrow C_2H_3*$	−0.97	0.54	1.51
R11	$(C_2H_3,H)* \rightarrow \beta\text{-}C_2H_4*$	2.13	3.65	1.52
R12	$H_2 + * \rightarrow H_2*$	0.00	-	-
R13	$H_2* \rightarrow (H,H)*$	−2.35	1.00	3.35
R14	$(H,H)*+\beta\text{-}C_2H_4* \rightarrow H* + (\beta\text{-}C_2H_4,H)*$	−0.01	-	-
R15	$(\beta\text{-}C_2H_4,H)* \rightarrow C_2H_5*$	−1.03	0.41	1.44
R16	$H* + C_2H_5* \rightarrow (C_2H_5,H)* + *$	−0.04	-	-
R17	$(C_2H_5,H)* \rightarrow C_2H_6 + *$	1.20	3.44	2.25
R18	$(C_2H_3,\beta\text{-}C_2H_2)* \rightarrow \delta\text{-}C_4H_5*$	−0.73	0.42	1.15

ethylene is 1.86 eV larger than for the dissociation of H_2 (eq R2), overall the TS of R7 lies approximately 1.2 eV below the TS of R2 in the reaction energy profile (Figure 6). This is consistent with the experimental fact that hydrogen splitting was the limiting step.

We also considered an alternative reaction pathway to eq R5 to form C_2H_3* species via the dissociative adsorption of acetylene (inset G in Figure 6) and the formation of a β-C_2H_2* isomer, a α-C_2H_2* radical species:

$$H_2 + (\beta\text{-}C_2H_2,H)* + H* \rightarrow H_2 + (C_2H,H,H)* + H* \quad \text{(R8)}$$

$$H_2 + (C_2H,H,H)* + H* \rightarrow H_2 + (\alpha\text{-}C_2H_2,H)* + H* \quad \text{(R9)}$$

$$H_2 + (\alpha\text{-}C_2H_2,H)* + H* \rightarrow H_2 + C_2H_3* + H* \quad \text{(R10)}$$

It is important to realize that, although this alternative pathway initially involves the thermodynamically preferred dissociative adsorption of acetylene (eq R8) releasing 1.73 eV, it is kinetically more energy-demanding than the pathway via β-C_2H_2* (eq R5). In particular, eq R8 is hindered by an activation energy of 0.74 eV, whereas in eq R5 the reaction proceeds almost without energy barrier (Table 1). Interestingly, it is the high reactivity of β-C_2H_2* species toward hydrogenation by nearby H* species what activates the formation of the key C_2H_3* species for the subsequent hydrogenation process, avoiding the thermodynamic preference for dissociative adsorption of isolated acetylene molecules.

Once a surface C_2H_3* species is formed, the reaction can proceed toward the formation and desorption of a gas-phase C_2H_4 molecule (eq R7), resulting in an overall partial hydrogenation process. Alternatively, the adsorbed C_2H_3 species can be hydrogenated to ethane via the formation of a β-C_2H_4* radical on the surface (inset I in Figure 6). The list of elementary steps leading to the complete hydrogenation process is:

$$H_2 + (C_2H_3,H)* + * \rightarrow H_2 + \beta\text{-}C_2H_4* + * \quad \text{(R11)}$$

$$H_2 + \beta\text{-}C_2H_4* + * \rightarrow H_2* + \beta\text{-}C_2H_4* \quad \text{(R12)}$$

dx.doi.org/10.1021/jp410478c | J. Phys. Chem. C 2014, 118, 5352–5360

$$H_2^* + \beta\text{-}C_2H_4^* \rightarrow (H,H)^* + \beta\text{-}C_2H_4^* \quad \text{(R13)}$$

$$(H,H)^* + \beta\text{-}C_2H_4^* \rightarrow H^* + (\beta\text{-}C_2H_4,H)^* \quad \text{(R14)}$$

$$H^* + (\beta\text{-}C_2H_4,H)^* \rightarrow H^* + C_2H_5^* \quad \text{(R15)}$$

$$H^* + C_2H_5^* \rightarrow (C_2H_5,H)^* + * \quad \text{(R16)}$$

$$(C_2H_5,H)^* + * \rightarrow C_2H_6 + 2^* \quad \text{(R17)}$$

Essentially, the reactions to form gas-phase C_2H_4 or β-C_2H_4* from C_2H_3* and H* species compete with each other (eqs R7 and R11, respectively). These two elementary steps present large energy barriers, but the pathway leading to gas-phase C_2H_4 is hindered by a substantially smaller activation energy, 2.86 eV, than the formation of β-C_2H_4*, 3.65 eV, which is kinetically less favorable (Table 1). The most energy-demanding step toward complete hydrogenation provides, therefore, an explanation to the experimentally observed strong ethylene selectivity. In addition, a selective catalyst is expected to offer a high (low) stability of adsorbed acetylene (ethylene), i.e., thermodynamic selectivity.[8] This qualitative requirement is actually consistent with our results. Comparing states I and F in Figure 6, the adsorption of gas-phase ethylene (state F) to form an activated adsorbed ethylene molecule on the surface (state I) is indeed an endothermic process by 0.5 eV, whereas the activation of a gas-phase acetylene to form a β-C_2H_2* species (state D) is slightly exothermic by 0.15 eV (eq R4). Therefore, a gas-phase ethylene molecule formed in eq R7 is not thermodynamically prone to be readsorbed on the surface.

Complete hydrogenation from C_2H_3* species through the formation of a β-C_2H_4* radical (eq R11) requires the physisorption and subsequent dissociation of a second H_2 molecule on the $CeO_2(111)$ surface (eqs R12 and R13). Coadsorbing H* and β-C_2H_4* species on nearby O surface atoms is thermo-neutral. The overall $(C_2H_3,H)^* + H^* \rightarrow (\beta\text{-}C_2H_4,H)^*$ process is slightly exothermic by 0.22 eV. The β-C_2H_4* radical can readily react with a nearby H* releasing 1.03 eV and with an activation energy of only 0.41 eV (eq R15). This process leads to the formation of very stable C_2H_5* species. Bringing together C_2H_5* and H* is slightly favorable by 0.04 eV (eq R16). Forming the final complete hydrogenation product, ethane, by the reaction of C_2H_5* with the coadsorbed H* (eq R17) is endothermic by 1.20 eV. In addition, this final hydrogenation step presents a large activation energy (3.44 eV), which hampers the reaction toward ethane and explains the very low selectivity to the overhydrogenated product observed experimentally.

As discussed before, the maximum selectivity to oligomers is actually higher than that to ethane (Figure 2a,b), and it is mostly ethylene participating in the production of oligomers (Figure 2c). Specifically, ethylene precursors (C_2H_3*) are very stable surface species, as pointed out by the corresponding deep potential well of state E in Figure 6. Hence, such species are expected to exhibit long resident times on the ceria surface. At low coverages, C_4 oligomers may result, for example, from direct coupling of C_2H_3* with a nearby β-C_2H_2* radical according to the following process:

$$(C_2H_3,\beta\text{-}C_2H_2)^* \rightarrow \delta\text{-}C_4H_5^* \quad \text{(R18)}$$

This reaction is moderately exothermic by 0.73 eV and is hindered by an activation energy of only 0.42 eV as shown in Table 1. Notice that the product of eq R18, δ-C_4H_5*, is a radical, which can presumably be release as a C_4 oligomer after reacting with nearby H* or evolve to a larger oligomer by attaching an extra C_xH_y* species, although such reaction pathways have not been explored here.

Interestingly though, compared with the formation of ethylene (eq R7), oligomerization via C_2H_3 and β-C_2H_2 recombination is largely preferred (Figure 7). It is important

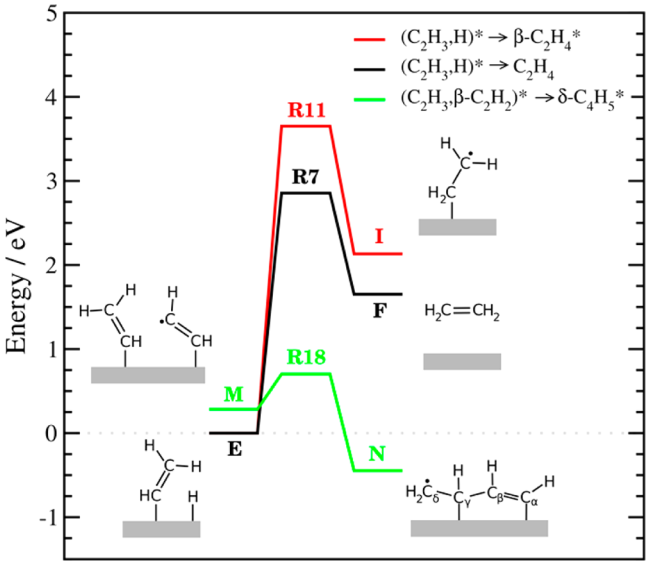

Figure 7. Reaction energy profile for the coupling of C_2H_3* and β-C_2H_2* (state M) into δ-C_4H_5* (state N) through eq R18 (green line). This process is compared with eq R7 (black line) and eq R11 (red line) in Figure 6. All energies are referenced to the total energy of $(C_2H_3,H)^*$ plus β-C_2H_2* systems (state E). States E, F, I, M, and N stand for minima and their structures are schematically shown in the insets, whereas transition structures are indicated by R7, R11, and R18 (see Figure S6 for more details).

to stress that each C_2H_x* species is surrounded by six nearby O surface atoms (Figure S6 in the Supporting Information); for oligomerization to occur, a second C_2H_x* species should be adsorbed on one of these six neighboring active sites, otherwise the separation between the two species is too large (>3.5 Å) for species to react. Since hydrogen competes for the same adsorption sites, the observed gradual decrease in oligomer production when increasing the H_2/C_2H_2 ratio can be linked to the fact that an excess of H* surrounding C_2H_x* species blocks the energetically more favorable oligomerization process, facilitating the conversion toward ethylene instead. This blocking effect is supported by the fact that surface H diffusion is hindered by a large energy barrier[45] and, therefore, H mobility is expected to be low even at high temperatures. We should emphasize that other oligomerization reactions could also be proposed. We have focused here only on the recombination of C_2H_3 and β-C_2H_2 (eq R18) because this is likely one of the most relevant oligomerization processes, but, for example, species such as β-C_2H_4* may actuate the oligomerization as well, which is expected to compete with ethane formation along the last steps of the complete hydrogenation process (from eq R11 to eq R17). A detailed study of oligomerization mechanisms is out of the scope of this work, however.

It is important to realize that the adsorption of C_xH_y* and H* intermediate species involves the reduction of the surface. It is precisely the ability of CeO_2 for easily accommodating one electron into Ce 4*f* states that facilitates the stabilization of β-

dx.doi.org/10.1021/jp410478c | J. Phys. Chem. C 2014, 118, 5352−5360

C_2H_2* radicals, a key reaction intermediate in the overall hydrogenation process. In addition, each elementary hydrogenation step (C_2H_xH)* → (C_2H_{x+1})* implies the reoxidation of a Ce^{3+} ion. Thus the reversibility of the $Ce^{4+} \leftrightarrow Ce^{3+}$ process is vital for understanding the outstanding hydrogenation properties of CeO_2.

As for the detrimental effect of oxygen vacancies on the reactivity, we find that all reactants and intermediate species involved in the reaction adsorbed on-top of surface O sites. Hence, the creation of oxygen vacancies upon strong pretreatment in H_2 at 673 K simply reduces the number of active sites.

5. CONCLUSIONS

Acetylene hydrogenation on polycrystalline ceria proceeds with very high selectivity to ethylene. Oligomers are the major byproduct (maximum 16%) and result from C−C couplings of C_2H_x* species. DFT simulations on $CeO_2(111)$ substantiate the experimental observations and provide molecular-level insight in the active sites and reaction mechanism. Ethylene formation is the reaction that is most likely to occur when C_2H_2 and H_2 are coadsorbed on neighboring surface oxygen sites of the $CeO_2(111)$ surface, as it is well favored over the formation of β-C_2H_4 radical species that would enable subsequent hydrogenation. Acetylene adsorption leads to the formation of highly reactive β-C_2H_2 radical species that are hydrogenated to form C_2H_3 with no barrier at large H_2/C_2H_2 ratios, and are likely to form oligomers at low ratios. Finally, the formation of ethane from C_2H_5 and H is endothermic with a significantly large barrier, rendering total hydrogenation an unfavorable reaction. We put forward that the key factor determining the outstanding performance of CeO_2 lies in its ability of stabilizing highly reactive β-C_2H_2 radicals on the (111) surface by easily accommodating one electron into Ce 4*f* states. This might provide a basis for understanding why other reducible oxides are not active in hydrogenation. The gathered atomic-level understanding of the reaction mechanism is of paramount importance for the future design of chemo and stereoselective CeO_2-based catalysts for the liquid-phase hydrogenation of triple bonds in polyfunctionalized substrates.

■ ASSOCIATED CONTENT

Supporting Information

Detailed DFT results (optimized coordinates, views of the optimized adsorbates and transition structures, as well as relative energies as a function of Ce^{3+} localization). This material is available free of charge via the Internet at http://pubs.acs.org.

■ AUTHOR INFORMATION

Corresponding Authors

*E-mail: jcarrasco@cicenergigune.com (J.C.).
*E-mail: jpr@chem.ethz.ch (J.P.-R.).

Author Contributions

The manuscript was written through contributions of all authors. All authors have given approval to the final version of the manuscript.

Notes

The authors declare no competing financial interest.

■ ACKNOWLEDGMENTS

We thank MINECO (CTQ2012-32928, MAT2011-23627, and CSD2010-00024) for financial support. Computer time provided by the SGAI-CSIC, CESGA, BIFI-ZCAM, University of Cantabria-IFCA, and the BSC is acknowledged. This work was granted access HPC resources made available within the Distributed European Computing Initiative by the PRACE-2IP, receiving funding from the EU's FP7 Programme under Grant Agreement No. RI-283493. J.C. is supported by the MINECO through a Ramón y Cajal Fellowship and acknowledges support by the Marie Curie Career Integration Grant FP7-PEOPLE-2011-CIG: Project NanoWGS and The Royal Society through the Newton Alumnus scheme. The COST action CM1104 is gratefully acknowledged. We thank Jörg Libuda for helpful discussions.

■ REFERENCES

(1) Rase, H. F. *Handbook of Commercial Catalysts: Heterogeneous Catalysts*; CRC Press: Boca Raton, 2000; p 110.
(2) Bartholomew, C. H.; Farrauto, R. J. *Fundamentals of Industrial Catalytic Processes*, 2nd ed.; Wiley: New York, 2005; p 411.
(3) Derrien, M. L. In *Catalytic Hydrogenation*; Červený, L., Ed.; Studies in Surface Science and Catalysis Series; Elsevier: Amsterdam, 1986; Vol. *27*, p 613.
(4) García-Mota, M.; Bridier, B.; Pérez-Ramírez, J.; López, N. Interplay between Carbon Monoxide, Hydrides, and Carbides in Selective Alkyne Hydrogenation on Palladium. *J. Catal.* **2010**, *273*, 92−102.
(5) García-Mota, M.; Gómez-Díaz, J.; Novell-Leruth, G.; Vargas, C.; Bellarosa, L.; Bridier, B.; Pérez Ramírez, J.; López, N. A Density Functional Theory Study of the 'Mythic' Lindlar Hydrogenation Catalyst. *Theor. Chem. Acc.* **2011**, *128*, 663−673.
(6) Teschner, D.; Borsodi, J.; Wootsch, A.; Révay, Z.; Hävecker, M.; Knop-Gericke, A.; Jackson, S. D.; Schlögl, R. The Roles of Subsurface Carbon and Hydrogen in Palladium-Catalyzed Alkyne Hydrogenation. *Science* **2008**, *320*, 86−89.
(7) Crespo-Quesada, M.; Yarulin, A.; Jin, M.; Xia, Y.; Kiwi-Minsker, L. Structure Sensitivity of Alkynol Hydrogenation on Shape- and Size-Controlled Palladium Nanocrystals: Which Sites Are Most Active and Selective? *J. Am. Chem. Soc.* **2011**, *133*, 12787−12794.
(8) Studt, F.; Abild-Pedersen, F.; Bligaard, T.; Sørensen, R. Z.; Christensen, C. H.; Nørskov, J. K. Identification of Non-Precious Metal Alloy Catalysts for Selective Hydrogenation of Acetylene. *Science* **2008**, *320*, 1320−1322.
(9) Bridier, B.; López, N.; Pérez-Ramírez, J. Molecular Understanding of Alkyne Hydrogenation for the Design of Selective Catalysts. *Dalton Trans.* **2010**, *39*, 8412−8419.
(10) Kyriakou, G.; Boucher, M. B.; Jewell, A. D.; Lewis, E. A.; Lawton, T. J.; Baber, A. E.; Tierney, H. L.; Flytzani-Stephanopoulos, M.; Sykes, E. C. H. Isolated Metal Atom Geometries as a Strategy for Selective Heterogeneous Hydrogenations. *Science* **2012**, *335*, 1209−1212.
(11) Vilé, G.; Bridier, B.; Wichert, J.; Pérez-Ramírez, J. Ceria in Hydrogenation Catalysis: High Selectivity in the Conversion of Alkynes to Olefins. *Angew. Chem., Int. Ed.* **2012**, *51*, 8620−8623.
(12) Segura, Y.; López, N.; Pérez-Ramírez, J. Origin of the Superior Hydrogenation Selectivity of Gold Nanoparticles in Alkyne Plus Alkene Mixtures: Triple- versus Double-Bond Activation. *J. Catal.* **2007**, *247*, 383−386.
(13) Guan, Y.; Hensen, E. J. M. Cyanide Leaching of Au/CeO_2: Highly Active Gold Clusters for 1,3-Butadiene Hydrogenation. *Phys. Chem. Chem. Phys.* **2009**, *11*, 9578−9582.
(14) Azizi, Y.; Petit, C.; Pitchon, V. Formation of Polymer-Grade Ethylene by Selective Hydrogenation of Acetylene over Au/CeO_2 Catalyst. *J. Catal.* **2008**, *256*, 338−344.

(15) Zhu, H.-Z.; Lu, Y.-M.; Fan, F.-J.; Yu, S.-H. Selective Hydrogenation of Nitroaromatics by Ceria Nanorods. *Nanoscale* **2013**, *5*, 7219−7223.
(16) Fronzi, M.; Soon, A.; Delley, B.; Traversa, E.; Stampft, C. Stability and Morphology of Cerium Oxide Surfaces in an Oxidizing Environment: A First-Principles Investigation. *J. Chem. Phys.* **2009**, *131*, 104701-1−104701-16.
(17) Branda, M. M.; Ferullo, R. M.; Causá, M.; Illas, F. Relative Stabilities of Low Index and Stepped CeO_2 Surfaces from Hybrid and GGA plus U Implementations of Density Functional Theory. *J. Phys. Chem. C* **2011**, *115*, 3716−3721.
(18) Sheth, P. A.; Neurock, M.; Smith, C. M. First-Principles Analysis of the Effects of Alloying Pd with Ag for the Catalytic Hydrogenation of Acetylene−Ethylene Mixtures. *J. Phys. Chem. B* **2005**, *109*, 12449−12466.
(19) López, N.; Bridier, B.; Pérez-Ramírez, J. Discriminating Reasons for Selectivity Enhancement of CO in Alkyne Hydrogenation on Palladium. *J. Phys. Chem. C* **2008**, *112*, 9346−9350.
(20) Bridier, B.; López, N.; Pérez-Ramírez, J. Partial Hydrogenation of Propyne over Copper-Based Catalysts and Comparison with Nickel-Based Analogues. *J. Catal.* **2010**, *269*, 80−92.
(21) Yang, B.; Burch, R.; Hardacre, C.; Hu, P. Origin of the Increase of Activity and Selectivity of Nickel Doped by Au, Ag, and Cu for Acetylene Hydrogenation. *ACS Catal.* **2012**, *2*, 1027−1032.
(22) Vilé, G.; Baudouin, D.; Remediakis, I. N.; Copéret, C.; López, N.; Pérez-Ramírez, J. Silver Nanoparticles for Olefin Production: New Insights into the Mechanistic Description of Propyne Hydrogenation. *ChemCatChem* **2013**, *5*, 3750−3759.
(23) Murgida, G.; Ganduglia-Pirovano, M. V. Evidence for Subsurface Ordering of Oxygen Vacancies on the Reduced CeO_2(111) Surface Using Density-Functional and Statistical Calculations. *Phys. Rev. Lett.* **2013**, *110*, 246101−1−246101−5.
(24) Ganduglia-Pirovano, M. V.; Hofmann, A.; Sauer, J. Oxygen Vacancies in Transition Metal and Rare Earth Oxides: Current State of Understanding and Remaining Challenges. *Surf. Sci. Rep.* **2007**, *62*, 219−270.
(25) Carrasco, J.; Barrio, L.; Liu, P.; Rodriguez, J. A.; Ganduglia-Pirovano, M. V. Theoretical Studies of the Adsorption of CO and C on Ni(111) and Ni/CeO_2(111): Evidence of a Strong Metal-Support Interaction. *J. Phys. Chem. C* **2013**, *117*, 8241−8250.
(26) Pacchioni, G. Modeling Doped and Defective Oxides in Catalysis with Density Functional Theory Methods: Room for Improvements. *J. Chem. Phys.* **2008**, *128*, 182505-1−182505-10.
(27) Castleton, C. W. M.; Kullgren, J.; Hermansson, K. Tuning LDA +U for Electron Localization and Structure at Oxygen Vacancies in Ceria. *J. Chem. Phys.* **2007**, *127*, 244704-1−244704-11.
(28) Plata, J. J.; Márquez, A. M.; Sanz, J. F. Communication: Improving the Density Functional Theory Plus U Description of CeO_2 by Including the Contribution of the O 2p Electrons. *J. Chem. Phys.* **2012**, *136*, 041101-1−041101-4.
(29) Ganduglia-Pirovano, M. V.; Da Silva, J. L. F.; Sauer, J. Density-Functional Calculations of the Structure of Near-Surface Oxygen Vacancies and Electron Localization on CeO_2(111). *Phys. Rev. Lett.* **2009**, *102*, 026101-1−026101-4.
(30) Jerratsch, J.-F.; Shao, X.; Nilius, N.; Freund, H.-J.; Popa, C.; Ganduglia-Pirovano, M. V.; Burow, A. M.; Sauer, J. Electron Localization in Defective Ceria Films: A Study with Scanning-Tunneling Microscopy and Density-Functional Theory. *Phys. Rev. Lett.* **2011**, *106*, 246801-1−246801-4.
(31) Li, H.-Y.; Wang, H.-F.; Gong, X.-Q.; Guo, Y.-L.; Guo, Y.; Lu, G.; Hu, P. Multiple Configurations of the Two Excess 4f Electrons on Defective CeO_2(111): Origin and Implications. *Phys. Rev. B* **2009**, *79*, 193401−1−193401−4.
(32) Paier, J.; Penschke, C.; Sauer, J. Oxygen Defects and Surface Chemistry of Ceria: Quantum Chemical Studies Compared to Experiment. *Chem. Rev.* **2013**, *113*, 3949−3985.
(33) Kresse, G.; Hafner, J. Ab-Initio Molecular-Dynamics for Liquid-Metals. *Phys. Rev. B* **1993**, *47*, 558−561.
(34) Kresse, G.; Furthmüller, J. Efficient Iterative Schemes for Ab Initio Total-Energy Calculations Using a Plane-Wave Basis Set. *Phys. Rev. B* **1996**, *54*, 11169−11186.
(35) The VASP site, http://www.vasp.at (version vasp.5.2.12).
(36) Kresse, G.; Joubert, D. From Ultrasoft Pseudopotentials to the Projector Augmented-Wave Method. *Phys. Rev. B* **1999**, *59*, 1758−1775.
(37) Dudarev, S.; Botton, G.; Savrasov, S.; Humphreys, C.; Sutton, A. Electron-Energy-Loss Spectra and the Structural Stability of Nickel Oxide: An LSDA+U Study. *Phys. Rev. B* **1998**, *57*, 1505−1509.
(38) Perdew, J.; Burke, K.; Ernzerhof, M. Generalized Gradient Approximation Made Simple. *Phys. Rev. Lett.* **1996**, *77*, 3865−3868.
(39) Fabris, S.; de Gironcoli, S.; Baroni, S.; Vicario, G.; Balducci, G. Reply to "Comment on 'Taming Multiple Valency with Density Functionals: A Case Study of Defective Ceria'". *Phys. Rev. B* **2005**, *72*, 237102-1−237102-2.
(40) Cococcioni, M.; de Gironcoli, S. Linear Response Approach to the Calculation of the Effective Interaction Parameters in the LDA+U Method. *Phys. Rev. B* **2005**, *71*, 035105-1−035105-16.
(41) Monkhorst, H. J.; Pack, J. D. Special Points for Brillouin-Zone Integrations. *Phys. Rev. B* **1976**, *13*, 5188−5192.
(42) Jónsson, H.; Mills, G.; Jacobsen, K. W. In *Classical and Quantum Dynamics in Condensed Phase Simulations*; Berne, B. J., Ciccotti, G., Coker, D. F., Eds.; World Scientific: Singapore, 1998; p 385.
(43) Molinier, M.; Ou, J. D. Y.; Risch, M. A. Hydrogenation Catalyst for Selective Hydrogenation of, e.g., Acetylene, Comprises Nickel- or Platinum-Based Component, Second and Third Metal or Metal-Based Component(s) from Specified Groups and Support and/or Binder. US2004/0176651 A1, 2004.
(44) The α refers to the first carbon that attaches to an surface O atom. By extension, the second carbon is the β carbon.
(45) Fernández-Torre, D.; Carrasco, J.; Ganduglia-Pirovano, M.; Perez, R. in preparation.
(46) Chen, H.-T.; Choi, Y. M.; Liu, M.; Lin, M. C. A Theoretical Study of Surface Reduction Mechanisms of CeO_2 (111) and (110) by H_2. *ChemPhysChem* **2007**, *8*, 849−855.